A computational model of the effects of macronutrients absorption and physical exercise on hormonal regulation and metabolic homeostasis

Maria Concetta Palumbo [a,*], Albert A. de Graaf [b], Micaela Morettini [c], Paolo Tieri [a], Shaji Krishnan [d], Filippo Castiglione [a,1]

[a] *Institute for Applied Computing (IAC) "Mauro Picone", National Research Council of Italy, via dei Taurini 19, Rome, 00185, Italy*
[b] *Department Healthy Living, Nederlandse Organisatie voor Toegepast Natuurwetenschappelijk Onderzoek (TNO), Sylviusweg 71, Leiden, 2333 BE, The Netherlands*
[c] *Department of Information Engineering, Università Politecnica delle Marche, via Brecce Bianche 12, Ancona, 60131, Italy*
[d] *Department Healthy Living, Nederlandse Organisatie voor Toegepast Natuurwetenschappelijk Onderzoek (TNO), Princetonlaan 6, Utrecht, 3584 BE, The Netherlands*

ARTICLE INFO

ABSTRACT

Regular physical exercise and appropriate nutrition affect metabolic and hormonal responses and may reduce the risk of developing chronic non-communicable diseases such as high blood pressure, ischemic stroke, coronary heart disease, some types of cancer, and type 2 diabetes mellitus. Computational models describing the metabolic and hormonal changes due to the synergistic action of exercise and meal intake are, to date, scarce and mostly focussed on glucose absorption, ignoring the contribution of the other macronutrients. We here describe a model of nutrient intake, stomach emptying, and absorption of macronutrients in the gastrointestinal tract during and after the ingestion of a mixed meal, including the contribution of proteins and fats. We integrated this effort to our previous work in which we modeled the effects of a bout of physical exercise on metabolic homeostasis. We validated the computational model with reliable data from the literature. The simulations are overall physiologically consistent and helpful in describing the metabolic changes due to everyday life stimuli such as multiple mixed meals and variable periods of physical exercise over prolonged periods of time. This computational model may be used to design virtual cohorts of subjects differing in sex, age, height, weight, and fitness status, for specialized in silico challenge studies aimed at designing exercise and nutrition schemes to support health.

1. Introduction

Unhealthy diets and physical inactivity contribute to the onset and/or progression of major non-communicable diseases, including diabetes, cardiovascular disorders, and certain types of cancer. Such behaviours substantially contribute to the global burden of disease, death, and disability [1].

In particular, diabetes mellitus was the sixth leading cause of disability in 2015 [2] and directly caused 1.5 million deaths worldwide in 2019 [3], as stated by the World Health Organization. The 10th edition of IDF Diabetes Atlas [4,5] estimates that in 2021, 537 million people are living with diabetes worldwide. For 2045, they predict that 783.2 million people will have diabetes. More than 90% of patients with diabetes have type 2 diabetes (T2D) [6]. T2D is a chronic condition characterized by insulin deficiency caused by pancreatic β-cell dysfunction and insulin resistance in target organs [6]. If intensive

lifestyle modifications, like diet and exercise, are not sufficient enough to properly manage the glycemia, pharmacotherapy may be necessary.

The wide intra- and inter-individual variability in response to treatments, drugs, and stimuli, leads the scientific research community to elaborate computational models to obtain cohorts of virtual diabetic patients in the view of personalized medicine approaches [7]. To date, mathematical/computational modeling efforts able to describe metabolic homeostasis in normal life conditions, which account for both nutritional regime and exercise, are quite limited. Adamu and coworkers [8] improved the model from Topp *et al.* [9] (who developed a model consisting in three nonlinear ordinary differential equations describing the dynamics of beta-cell mass, insulin, and glucose) taking into account the number of calories ingested after a meal or burnt through exercise, a not obvious quantity to measure. Svitra and colleagues presented a model consisting of a predator–prey ordinary

differential equations system with a delay, representing normal and diabetic subjects by means of two periodic functions defining both nutrition and exercise [10]. Breton *et al.* proposed a "parsimonious" model of the effects of exercise on glucose homeostasis that links the change in insulin action and glucose effectiveness to the heart rate [11]. This last work was used in a large-scale simulation model of glucose metabolism in type 1 diabetes by Dalla Man and coworkers to simulate daily life conditions including both nutrition and physical activity [12]. Balakrishnan and colleagues developed a hybrid model for type 1 diabetes (T1D) patients [13] in which they modeled the exercise intensity using a variable that defines the level of physical exertion an individual feels during exercise. In this work, the body weight is the only customizable factor as regards the subjects' characteristics. Resalat *et al.* and Islam *et al.* proposed mathematical models to represent different kinds of in-silico virtual patient populations for T1D [14] and T2D [15]. Resalat and coworkers [14] introduced two single and dual hormone mathematical models that represent an in-silico virtual patient population. The single hormone comprises differential equations describing insulin dynamics and carbohydrate absorption. The dual hormone virtual patient population incorporates additional equations representing glucagon dynamics. The study by Islam [15] aimed to build a constraint-based comprehensive model of glucose dynamics to describe insulin-independent (type-2) diabetes and also plasma glucose variation over carbohydrate ingestion, insulin injection, and exercise sessions. The model consists of seven compartments, connected by a "plasma" compartment. Deichmann *et al.* proposed a model for T1D patients in which the physical activity was considered via accelerometer count and the meal ingested consists of a dose of glucose [16]. Sarkar *et al.* realized a multi-scale model, spanning from cellular processes, distinct organs and whole-body features, including the effects of meal consumption and physical exercise [17]. The meals are represented by their caloric content, and the effects of physical activities are incorporated into the model, without explicitly modeling it. More recently Kurata [18] has proposed a multi-organ and multi-scale virtual metabolic human dynamic model that captures key features of whole-body metabolism and simulates the dynamics of essential metabolites after a meal composed of glucose and triglycerides. The model was validated under healthy and disease condition, however it is not designed to describe the effects of physical exercise and does not explicitly model the metabolic control by the key hormone epinephrine. Other parsimonious models have been developed to describe the contribution of non-esterified fatty acids or amino acids on insulin secretion following a meal [19,20].

In a previous work, we have proposed a multi-scale computational model for whole body fuel homeostasis [21] during exercise. Notably, such a model is inspired by the work by Kim *et al.* [22] and includes the description of the metabolic and hormonal changes due to a bout of exercise by using the definition of "relative" (rather than absolute, thus fixed) exercise intensity as well as the estimation of functional capacity about age, gender, anthropometric characteristics, and current fitness status, to achieve greater generalization and user-customization. Moreover, we modeled the oxygen consumption and the dynamics of epinephrine as directly dependent on the relative exercise intensity to modulate the hormones and the glucose responses. Here we aim to extend our previous computational model [21] to account for the description of the metabolic and hormonal status by also considering the effects of meal consumption to realize a tool able to represent the fuel homeostasis in real life condition, depending on the lifestyle and daily habits. The main novelty here introduced is the modeling of the food intake, stomach emptying and gut absorption of all three macronutrients (proteins, carbohydrates, fats).

Table 1
List of model input parameters.

Parameter	Meaning
Gender	male/female
Age	age (years)
BW	body weight (kg)
T_v	target value of exercise intensity (%VO$_{2max}$)
fitness status	cardio-respiratory fitness level (from "poor" to "superior") [23]
t_{ex}^{start}, t_{ex}^{end}	start/end of the exercise session (min)
t_{meal}^{start}	meal start (min)
D_{glu}	dose of glucose from ingested grams of carbohydrates
D_{ala}	dose of alanine from ingested grams of proteins
D_{tg}	dose of triglycerides from ingested grams of fats

2. Methods

The whole body model is composed of seven tissue compartments, namely *heart*, *skeletal muscle*, *liver*, *gastrointestinal tract*, *adipose tissue*, *brain* and *other tissues*. Each compartment is described by dynamic mass balances and major cellular metabolic reactions, as in the original model by Kim *et al.* [22].

In Section 2.1 we introduced a model of nutrient intake, stomach emptying and absorption of macronutrient monomers in the gastrointestinal (GI) tract. The glucagon–insulin model is incorporated into the whole-body model to predict hormonal changes during a meal in addition to those taking place during exercise, which was already described in the previous implementation [21]. After meal ingestion, blood glucose concentration changes and, consequently, the plasma concentrations of insulin and glucagon are subject to physiological modifications, leading to the maintenance of the glucose homeostasis, as described in Section 2.2. The implementation of the nutrition intake and processing model leads to a multi-regime dynamic model for the simulation of the whole-body fuel homeostasis, as depicted in Fig. 1.

The input parameters of this model are listed in Table 1.

The model has been coded in ANSI C computer language to achieve maximal performance and portability. The differential equations are solved numerically with the CVODE library, a solver for stiff and nonstiff ordinary differential equation systems [24,25].

2.1. Modeling food intake, stomach emptying and gut absorption

Meal consumption comprises the following two processes: (i) nutrients intake (*i.e.,* orally ingested food) and stomach emptying; (ii) absorption of macronutrients carbohydrates (represented as glucose in the model), proteins (represented as amino acids), and fats (as triglycerides). To translate such processes into the model, we implemented three main steps: nutrient quantities conversion, gastric emptying, and appearance in the GI tract, as shown in Fig. 2.

Output values from the GI then feed the liver compartment, as shown in Fig. 1. The model inputs consist of grams of carbohydrates (CHO), proteins, and fats. The processes and calculations describing the phases of food intake, from the oral ingestion to the gastrointestinal absorption of macronutrient monomers, are detailed as follows.

As a first step, we converted the grams of macronutrients (carbohydrates, proteins, and fats) into their millimole equivalents of the respective macronutrient monomers (glucose, alanine, and triglycerides). For convenience, in the model CHO are reduced to the equivalent number of glucose monomers. Considering that proteins represent a minor contribution to energy metabolism compared to carbohydrates and lipids, amino acids are represented solely by alanine, as also done in [22]. Likewise, all proteins are reduced to the equivalent number of alanine monomers; and trioleate (a triglyceride derived from glycerol and three units of the unsaturated fatty acid oleic acid) is the representative dietary triglyceride (or triacylglycerol), because oleic acid is the most abundant fatty acid in most vegetable oils [26].
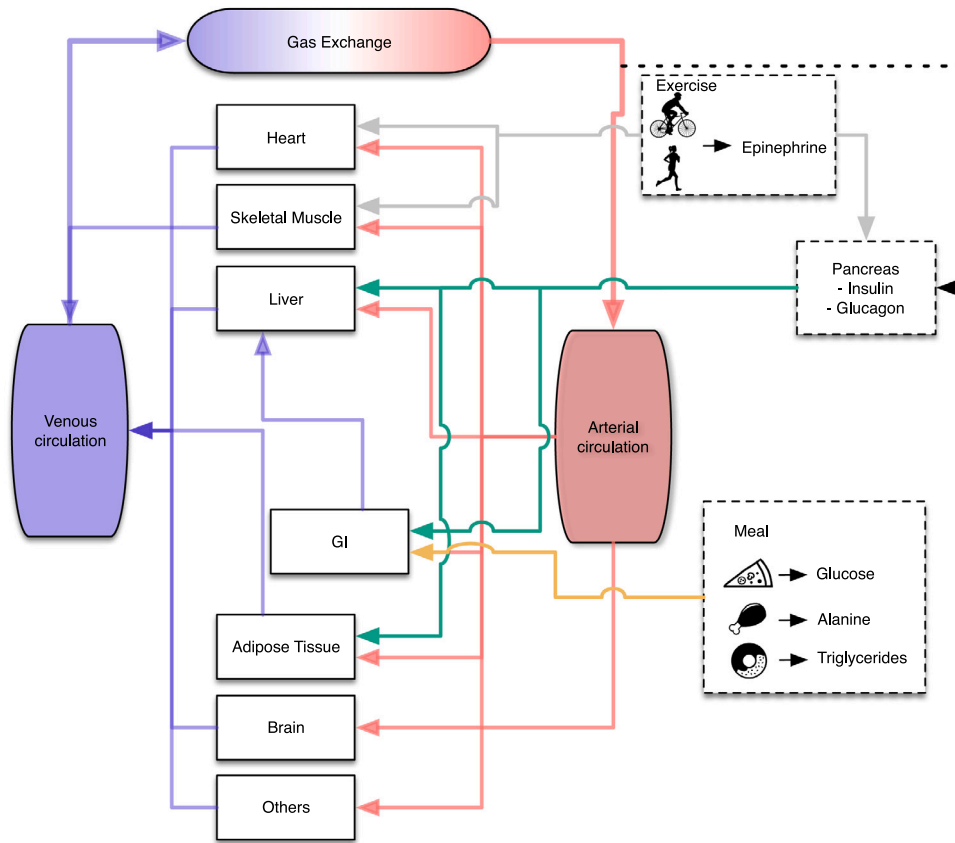
Fig. 1. Whole body system diagram. Exercise stimulates epinephrine release which influences the pancreatic secretion of insulin and glucagon and acts as a neuroendocrine signal for the heart and skeletal muscle (gray lines). Meal intake and macronutrient absorption modify the metabolic flux rates of glucose, alanine, and triglycerides in the GI compartment (orange line). The arterial/venous circulation (red/purple lines) connects each organ. Arterial glucose concentration (dotted line) signals the pancreas to set the levels of insulin and glucagon, whose ratio influences metabolic reaction rates in the liver, GI tract, and adipose tissue (green lines). Three ordinary differential equations are added to the previous model [21] to describe the food intake leading to a total of 139 ordinary differential equations in the multi-scale computational model.
Source: Adapted from [22].
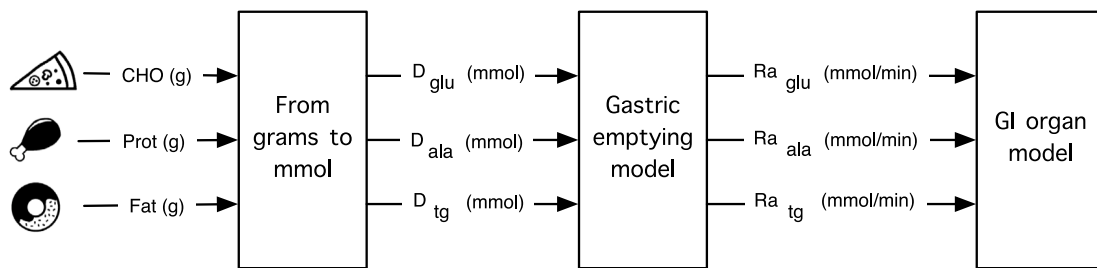
Fig. 2. Main processes and calculations involved in modeling food intake, stomach emptying, and gut absorption. Quantities (grams) of carbohydrates (CHO), proteins (Prot), and fats (Fat) ingested are converted into their millimole equivalent of glucose (D_{glu}), alanine (D_{ala}), and triglycerides (D_{tg}). Then, the gastric emptying model provides the rates of appearance Ra_{glu}, Ra_{ala}, Ra_{tg} of glucose, alanine, and triglycerides, which enter the GI compartment.

As for the conversion factors, we used molar weights (MW) of monomer glucose (180 g/mol), of trioleate (884 g/mol) and of alanine (71 g/mol). As an example, for glucose ("glu") the conversion is

$$D_{glu} = \frac{CHO}{MW_{glu} \cdot 1000}.$$

To formulate the equations introducing stomach emptying and gut nutrient absorption into the model, we followed the studies by Dalla Man *et al.* [27] and Elashoff *et al.* [28]: the amount of nutrient n (n stands for glucose from CHO, alanine from proteins, and triglycerides from fats) emptied in the duodenum, increases following a power exponential function given by

$$q_{duo}(t, n) = D_n \cdot (1 - e^{(-(K_{e,n} \cdot t)^{\beta_n})}) \tag{1}$$

with D_n being the nutrient dose in mmol given into the stomach, $K_{e,n}$ a kinetic constant, and β_n a shape factor depending on the meal type in

Table 2
Parameters used to model the meal intake. List of model parameters for stomach emptying and absorption of glucose (glu), alanine (ala) and triglycerides (tg).

Parameter	Value for OGTT	Value for mixed meal	Units
β_{glu}	1.23 [27]	1.05	
β_{ala}		1.6	
β_{tg}		2.2	
$K_{e,glu}$	0.011 [27]	0.0164	min^{-1}
$K_{e,ala}$		0.0086	min^{-1}
$K_{e,tg}$		0.0042	min^{-1}
$K_{abs,glu}$	0.231 [27]	0.021	min^{-1}
$K_{abs,ala}$		0.013	min^{-1}
$K_{abs,tg}$		0.017	min^{-1}
$F_{abs,glu}$	0.9 [27]	0.9	
$F_{abs,ala}$		0.95	
$F_{abs,tg}$		0.95	

which the nutrient is present. For liquid meals β_n=1, whereas for solid meals it may range up to 2 or even beyond. $K_{e,n}$ (expressed in min^{-1}) is related to the stomach emptying half-time $t_{1/2}$ as follows:

$$K_{e,n} = exp \left(ln(ln(2))/\beta_n - ln(t_{1/2}) \right). \tag{2}$$

Taking the derivative of Eq. (1), the gastric emptying rate $G_{emp,n}(t)$ for nutrient n is

$$G_{emp,n}(t) = D_n \cdot \beta_n \cdot K_{e,n}^{\beta_n} \cdot t^{(\beta_n-1)} \cdot e^{-(K_{e,n} \cdot t)^{\beta_n}}$$

The equations describing first-order kinetics of glucose absorption and rate of appearance are given below:

$$\begin{cases} dy_{n(t)}/dt = -K_{abs,n} \cdot y_n(t) + G_{emp,n}(t) \\ Ra_n(t) = F_{abs,n} \cdot K_{abs,n} \cdot y_n(t) \end{cases} \tag{3}$$

in which $y_n(t)$ is the amount of nutrient n in the gut (expressed in mmol), $K_{abs,n}$ (in min^{-1}) represents the rate constant of intestinal absorption, Ra_n (in mmol/min) is the rate of appearance of the nutrient in the gut and $F_{abs,n}$ describes the fraction of intestinal absorption which actually appears in plasma. Finally, we added a quantity equal to $Ra_n/V_{eff,n,GI}$ to the concentration of the nutrient in the model of the GI, in which $V_{eff,n,GI}$ (in l) describes the effective distribution volume of the nutrient in the gut compartment, according to the original model by Kim [22]. Since the model in [21] works with perfectly mixed lumped tissue-capillary compartments (as per the assumptions made by Kim in [22]), it will automatically generate the correct sign for metabolite transfer from the GI into the portal plasma compartment. The implementation of the model describing the dynamics of alanine ("ala") and triglycerides ("tg") during meals, needs proper parameters (*i.e.*, β_{ala}, β_{tg}, $K_{e,ala}$, $K_{e,tg}$, $K_{abs,ala}$, $K_{abs,tg}$, $F_{abs,ala}$ and $F_{abs,tg}$) listed in Table 2, whose setting is described in the following Section.

Parameter setting for stomach emptying and macronutrient absorption

The procedure to find the model parameters in Table 2 comprises the following steps for the three different nutrients:

1. determine values for the shape factor β_n in Eqs. (1) and (2);
2. determine values for stomach half-emptying time $t_{1/2}$;
3. calculate $K_{e,n}$ values by substituting the results of step 1 and 2 in Eq. (2);
4. determine $K_{abs,n}$ values for the different nutrients using Eq. (3) with reported nutrient absorption data $Ra_n(t)$;
5. estimate absorption fractions $F_{abs,n}$.

Shape factor β_n. Non-liquid meals will come with an Elashoff shape factor $\beta > 1$ [28]. For carbohydrate (glucose) meals, literature values of on average 1.05 are reported in [27,28]. For mixed meals, β values between 1.3 and 2.2 are reported [28–31]. We took a value of 2.2 (*i.e.*,

the higher extreme) as a likely representative value for nutrient fat (triglycerides). Low fat-containing meals show lower values for β [30] so we took the lower reported value *i.e.,* $\beta = 1.6$ as probably being representative for the nutrient protein (alanine).

Stomach half-emptying time $t_{1/2}$. The prediction of the stomach half-emptying time $t_{1/2}$ for a given mixed meal is a challenging task simply because there are so many factors that influence gastric emptying. In a pragmatic approach we made use of caloric density values to fix the stomach half-emptying time. This choice is based on the paper by Calbet and MacLean [32], where the following relation for $t_{1/2}$ was observed for liquid meals:

$$t_{1/2} = 9 + 27.5 \cdot d \tag{4}$$

where d is the caloric density of the meal expressed in kcal/ml. This implies that the amount of liquid taken with a meal can strongly influence $t_{1/2}$.

A difficulty arises if $\beta > 1$, because the meal cannot be considered a liquid meal anymore and the Calbet proportionality of Eq. (4) may not hold. Since a systematic study similar to Calbet's for solid meals of different compositions is lacking, we estimated the nutrient-specific $t_{1/2}$ values for carbohydrates, proteins, and fats by assuming that the gastric emptying of each nutrient in the meal still behaves according to Eq. (4), governed by the nutrient-specific caloric density. Since the caloric density d is modulated by the liquid components of the meal, we reasoned to which extent the different nutrients are expected to dissolve in the stomach. Meal carbohydrates are often present as rapidly dissolving sugars, *i.e.,* the carbohydrate caloric density is reduced by any drink taken with the meal. We pragmatically assumed a factor of 5 caloric density reduction for carbohydrates. Meal protein will be diluted mainly by acid gastric juices and to a lesser extent by the drinks. We therefore assumed a protein caloric density reduction by a factor of 2 in meals. Meal fat will form an emulsion by the action of gastric juices, resulting in only a slight reduction of caloric density which we assumed to be 1.25.

We computed the nutrient caloric densities d (kcal/ml) required in Eq. (4) by dividing the reported caloric contents of the solid (or pure) nutrient by our mentioned above reduction factors, *e.g.,* 5 for carbohydrates, 2 for proteins and 1.25 for fats. The caloric density is given by the product of the caloric content and the density of the nutrient, thus giving

$$d = \frac{caloric\ content \cdot density}{reduction\ factor}.$$

We used reference values for caloric content and density of carbohydrates, proteins and fats available from the internet [33] obtaining the following values:

- carbohydrates (sucrose): 4.1 kcal/g (caloric content), 1.5 g/ml (density);
- proteins: 4.1 kcal/g (caloric content), 1.4 g/ml (density);
- fats (tripalmitin, triolein, olive oil): 9.3 kcal/g (caloric content), 0.9 g/ml (density).

After applying the pragmatic reduction factors, the Calbet proportionality in Eq. (4) yields $t_{1/2}$ values of 43, 88, and 193 min for carbohydrates, proteins, and fat, respectively.

Stomach emptying of mixed meals is a complex process whose accurate description is beyond the scope of this work. Very briefly, liquid components will empty first, then semi-liquids, and finally the fat, which float on top of the other nutrient mixtures in the stomach. The obtained $t_{1/2}$ values match well with this description.

Stomach emptying rate constants $K_{e,n}$ Substituting the β and $t_{1/2}$ values reported above in Eq. (2), yields $K_{e,glu} = 0.0164$ min^{-1}, $K_{e,ala} = 0.0086$ min^{-1} and $K_{e,tg} = 0.0042$ min^{-1}.

Table 3

Estimation of gut absorption kinetic constants for proteins and fats versus CHO using Eq. (5), based on gut perfusion data from Table 3 and 4 in Weber *et al.* [34].

	Absorptive capacity	Perfusion rate at half max absorption	Perfusion rate	Perfusion rate constant
	V_{max} (kcal min^{-1} m^{-1})	K_m (kcal min^{-1})	S (kcal min^{-1})	K_{perf} (m^{-1})
meal C				
CHO	0.62	0.67	0.74	0.44
protein	0.2	0.18	0.32	0.4
fat	0.5	0.79	0.32	0.45
meal P				
CHO	0.52	0.57	0.24	0.64
protein	0.27	0.04	0.89	0.29
fat	0.27	0.42	0.24	0.41
meal E				
CHO	0.48	0.49	0.42	0.53
protein	0.18	0.01	0.55	0.32
fat	0.33	0.34	0.41	0.44
Average K_{perf}				
CHO				0.53
protein				0.33
fat				0.43

Table 4

Experimental datasets used for model validation.

Study	Population			Observables	
	n	Age (yrs)	BMI (kg m^{-2})	Hormone	Metabolites fluxes and concentrations
van Schalkwijk [35] (M)	5 ubo	48	28.7	INS	GLU, FFA, GLR, TG
	7 lbo	52	28.4	INS	GLU, FFA, GLR, TG
Dalla Man [36] (M)	100	55	26.6	INS	GLU, Ra$_{glu}$
Short [37] (M+E)	11	26	26.4	INS	GLU, FFA
Reaven [38] (M)	9	52	26.8	INS	GLU, FFA, LAC
Vors [39] (M)	9 ob	30	31.7	INS	FFA, Ra$_{tg}$
	9 nw	28	22.3		
Groen [40] (M)	20	23	22.6		Ra$_{ala}$

BMI: body mass index; M: meal test; M+E: meal test + exercise; lbo: lower body obese subjects; ubo: upper body obese subjects; ob: obese subjects; nw: normal weight subjects; INS: insulin; GLU: glucose; Ra$_{glu}$: glucose rate of appearance; FFA: free fatty acids; GLR: glycerol; TG: triglycerides; Ra$_{tg}$: triglycerides rate of appearance; Ra$_{ala}$: alanine rate of appearance.

Rate constants of intestinal absorption $K_{abs,n}$. In human food-absorption studies, absorption is often mistaken for gastric emptying kinetics and metabolism. For this reason, we have struggled to derive values for intestinal absorption rate constants from published human study data, except for glucose studied in more detail. However, a very instructive work by Weber and Ehrlein [34] describes the study of macronutrient absorption *in situ* in mini pigs, often used as a model for humans in nutrition kinetics studies. That paper analyzed the nutrient absorption of a gut segment using Michaelis–Menten kinetics. It shows that the nutrient absorption V_{max} and K_m values were dynamically changed by the gut depending on the overall macronutrient composition of a meal. The authors took into consideration the caloric contents of food, which fits well with our approach in which stomach emptying $t_{1/2}$ is also based on caloric content. The authors also specified the length, but not the surface area of the gut segment they used, which would otherwise have allowed us to translate V_{max} more easily to the human case: in fact, since area estimates for human duodenum, jejunum, and ileum gut sections are known, we could have directly obtained the parameter V_{max} for our setting. Another difficulty is that Weber and colleagues used a different type of kinetics, *i.e.,* Michaelis–Menten instead of first-order exponential. Moreover, the dimensions used are not the usual molar flux and concentration units, but instead perfusion rates. To overcome this problem, we resorted to the following pragmatic approach to derive the absorption rate constant $K_{abs,n}$ values from the data in Weber *et al.* [34]: information in Tables 3 and 4 of the above mentioned paper are used to derive perfusion-based first-order reaction rate constants $K_{perf,n}$ values of carbohydrates, proteins,

and fats, which are then calibrated to nutrient absorption rate constants values using literature $K_{abs,glu}$ values for glucose as a reference. The first step consists of simply equating the Michaelis–Menten flux reported by Weber *et al.* to the product of $K_{perf,n}$ and the nutrient perfusion rate S (effectively treating the perfusion as exponential kinetics) for each nutrient separately:

$$V_{max} \cdot \frac{S}{S + K_m} = K_{perf,n} \cdot S$$

thus resulting in:

$$K_{perf,n} = \frac{V_{max}}{S + K_m}. \tag{5}$$

The resulting $K_{perf,n}$ values for three different meal perfusions are shown in Table 3.

The average $K_{perf,n}$ values obtained from Table 3 are 0.53 m^{-1} for carbohydrates, 0.33 m^{-1} for proteins and 0.43 m^{-1} for fats. From this, we inferred that kinetic constants for nutrient absorption $K_{abs,n}$ will have the same relative magnitudes, *i.e.,* $K_{abs,ala}$ for protein approximately 63% that of carbohydrates, and $K_{abs,tg}$ for fat approximately 81% of that for carbohydrates (all in terms of calories).

To obtain absolute values, we used data from Dalla Man [27], who analyzed plasma glucose appearance curves with four different models and report $K_{abs,glu}$ values for glucose from meals in the range of 0.011 to 0.198 min^{-1}. A weighted average considering the reported coefficients of variation for the parameters of the four models reported in the work by Dalla Man [27] yields $K_{abs,glu} = 0.021$ min^{-1}. From that,
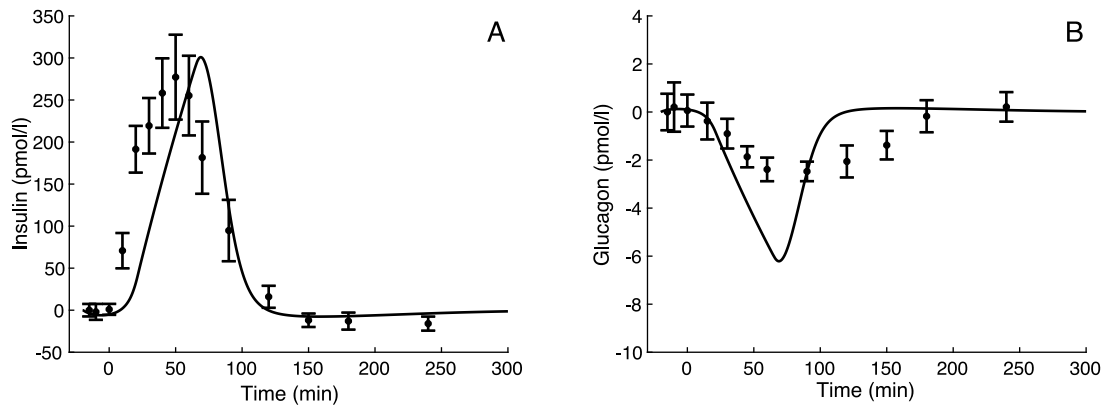
Fig. 3. Dynamics of suprabasal insulin and glucagon levels. Model fit (solid line) vs experimental data (circles), expressed as mean ± SE from the study by Knop [41]. The OGTT is administered at time 0. A: Insulin. B: Glucagon.

for protein (alanine) we estimated $K_{abs,ala}$ as 0.013 min^{-1} and for fat (triglycerides), $K_{abs,tg}$, is estimated as 0.017 min^{-1}.

Absorption fractions $F_{abs,n}$. The GI tissue actively uses the glucose. Hence $F_{abs,glu}$ is estimated to be 0.9. We postulated a value of 0.95 for $F_{abs,ala}$ and $F_{abs,tg}$ consistent with a less active GI tissue metabolism of proteins and fats. We assumed the removed fractions totally oxidized to carbon dioxide, that is, the metabolic products are not further considered.

2.2. Improvements to the hormonal glucagon/insulin model

The dynamics of glucagon and insulin during the meal period is given by the following differential equations:

$$\frac{dC_I}{dt} = C_I(t) \cdot \left[\psi \cdot [h - k_3 \cdot (C_G(t) - C_{G,0}) - k_4 \cdot (C_I(t) - C_{I,0}) - k_5 \cdot (C_E(t) - C_{E,0})] - D \right] \quad (6)$$

$$\frac{dC_G}{dt} = C_G(t) \cdot \left[\phi \cdot [h - k_1 \cdot (C_G(t) - C_{G,0}) - k_2 \cdot (C_I(t) - C_{I,0})] - D \right] \quad (7)$$

in which $C_I(t)$, $C_G(t)$ and $C_E(t)$ are the insulin, glucagon and epinephrine blood concentrations. Their basal values ($C_{I,0}$, $C_{G,0}$ and $C_{E,0}$ respectively), as well as h and parameters ϕ and ψ, are taken from the original model [22]

$$\phi = \begin{cases} 1 & C_{a,glc} < 2.5 \\ 1 - (C_{a,glc} - 2.5)^2/25 & 2.5 \leq C_{a,glc} \leq 7.5 \\ 0 & C_{a,glc} > 7.5 \end{cases} \quad (8)$$

$$\psi = \begin{cases} 0 & C_{a,glc} < 2.5 \\ 1 - (C_{a,glc} - 7.5)^2/25 & 2.5 \leq C_{a,glc} \leq 7.5 \\ 1 & C_{a,glc} > 7.5. \end{cases} \quad (9)$$

The value for the parameter k_5 in Eq. (7), accounting for the contribution of the exercise, can be found in [21] ($k_5 = 3.6 \cdot 10^{-5} \text{pM}^{-1} \text{min}^{-1}$).

Since in this work we introduced the new operation regime of food digestion that is different from the one represented by the physical exercise (and described in [21]), a new set of parameters (k_1, k_2, k_3, k_4, D) for the glucagon/insulin model different from those used for the exercise regime is estimated. As a consequence, the time periods of the exercise sessions and the prandial period cannot overlap. We found the conditions corresponding to out-of-meal and out-of-exercise by setting the Ra_n and y_n equal to zero (Eq. (3)) and using the same parameters (k_1, k_2, k_3, k_4, D) as in the meal period. We assumed the duration of the meal absorption limited to 180 min. Since this duration cannot account for the absorption of large meals, we added correction factors to consider the absorption of macronutrients beyond the 180 min interval. In other words, meal calories are absorbed in 180 min, and after that period, Ra_n=0. We used correction factors to rescale the area under the curve (AUC) of the three Ra_n computed at

180 min to equate them to the respective total AUC computed when the total absorption is achieved and the curves return to zero.

For the estimation procedure, we used experimental data of glucose, glucagon, and insulin plasma concentrations from a 50 g oral glucose tolerance test (OGTT) study conducted by Knop and colleagues in [41] in which blood samples are drawn from 10 healthy control subjects before, during, and 4 h after the test. This study provides a large set of experimental data for the hormones and glucose concentrations, allowing to estimate the five unknown parameters.

The Eqs. (6)–(7) describing the glucagon/insulin model depend on the glucose arterial concentration via ϕ and ψ, as illustrated in Eqs. (8)–(9). As a consequence, the first necessary step to the estimation procedure is to find a function describing the glucose kinetics by fitting the glucose experimental data during the test meal (see Appendix Modeling glucose dynamics during an OGTT study for further details). Afterward, we used the function describing the glucose kinetics as input of the glucagon/insulin model to estimate the parameters k_1, k_2, k_3, k_4, D, to retrieve the dynamics of glucagon and insulin during the meal period.

We performed parameter estimation using a weighted non-linear least squares approach, based on the Levenberg–Marquardt algorithm for the minimization procedure implemented in the "lsqnonlin" MATLAB®(The MathWorks, Natick, MA, USA) function. The differential equations of the model are solved using the "ode15s" MATLAB function, an implicit integration algorithm for stiff systems of equations. The precision of the estimate of each parameter is expressed using the percent coefficient of variation, $CV\% = (SD_e/e)$, where the standard deviation SD_e is derived from the inverse of the Fisher information matrix and e is the corresponding parameter estimate [42]. The errors in the glucagon and insulin measurements are assumed to be normally distributed random variables, with zero mean and a constant percent coefficient of variation equal to 4%.

2.3. Data for model validation

The refined model of the combined effect of food digestion and exercise on human metabolism is validated against experimental data (regarding hormones and metabolites fluxes and concentrations) from independent studies on healthy individuals in fasted conditions [35–40,43]. Details for each study are reported in Table 4 and in the Appendix "Data regarding the experimental studies used for validation".

3. Results

In Section 3.1, we reported the results of the parameter estimation procedure (described in Section 2.2). In Section 3.2 we reported the
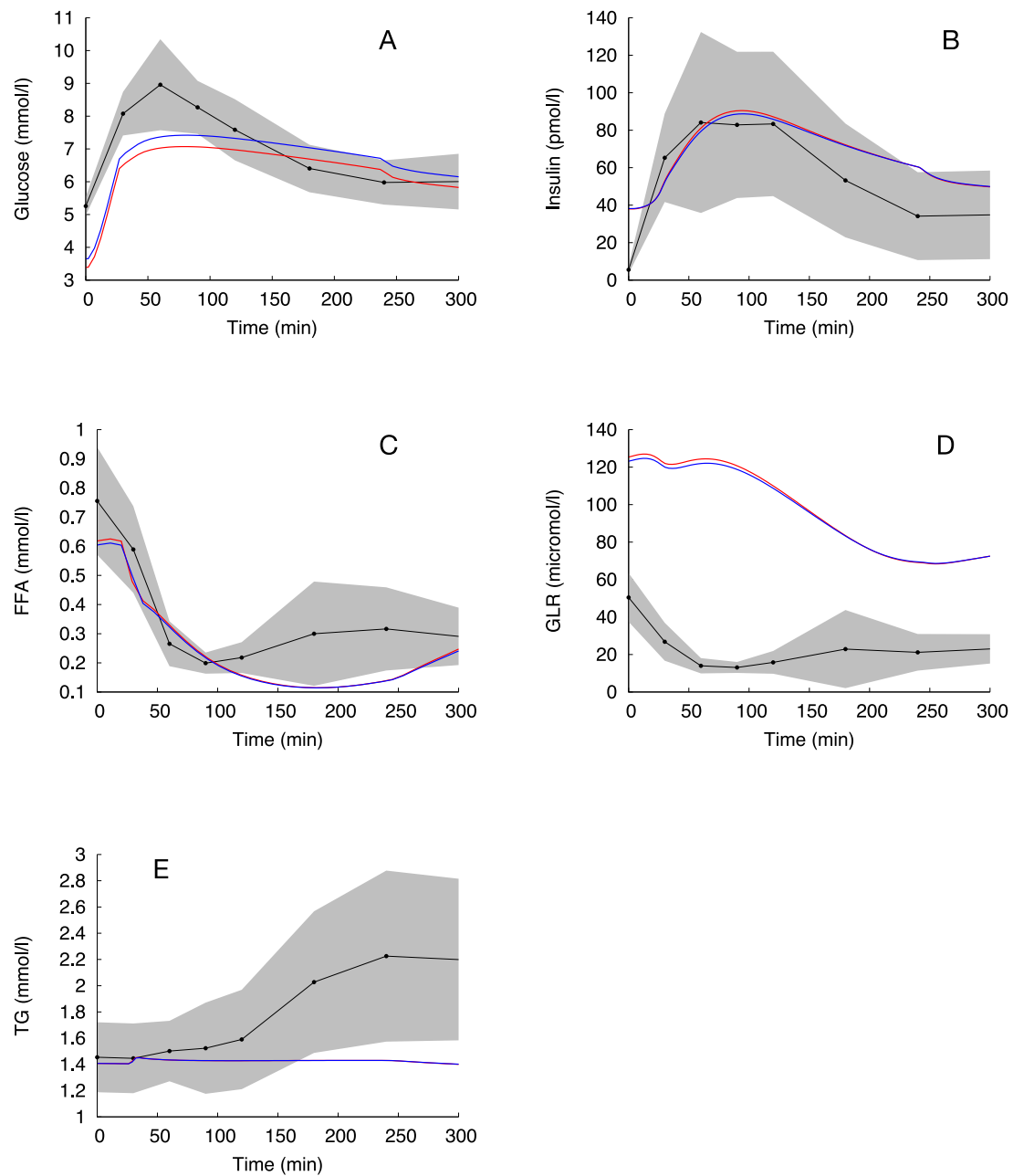
Fig. 4. Dynamics of metabolites in response to the meal test. Model fit vs experimental data, from the study by van Schalkwijk [35] during and after the trial for LBO (red line) and UBO (blue line) patients. The gray area represents the range of variability of the mean experimental data (black line). A: Glucose. B: Insulin. C: Free Fatty Acids (FFA). D: Glycerol (GLR). E: Triglycerides (TG).

results of the validation of our model by comparing simulated dynamics to experimental reference data on hormones and metabolites obtained from independent studies (see Section 2.3).

3.1. Estimated parameters

Table 5 summarizes the estimated parameters k_1, k_2, k_3, k_4, D of the glucagon/insulin model, along with their CV%, obtained by applying the procedure in Section 2.2. The R^2 (and the related p-values) are, respectively, 0.69 (0.0002) for insulin and 0.50 (0.0097) for glucagon.

The dynamics of the hormones resulting by using the estimated parameters on the mean of the experimental data are reported in Fig. 3.

3.2. Model validation

Results of the validation for the experimental datasets described in Table 4 are reported in Figs. 4–8.

For what concerns the simulated concentrations of glucose (Panels A in Figs. 4, 6, 7, Panel B in Fig. 5) and insulin (Panels A in Figs. 5, 8, Panels B in Figs. 4, 7 and Panel C in Fig. 6), the trends, the amplitudes and the timing of the peaks are, in general, coherent with the range of variability of the measured values in the case of both single and multiple meal tests. However, our model tends to underestimate the levels of glucose after the overnight fast and the peak amplitude of insulin. The decrease of FFA (Panel B in Fig. 8, Panel C in Figs. 4, 7
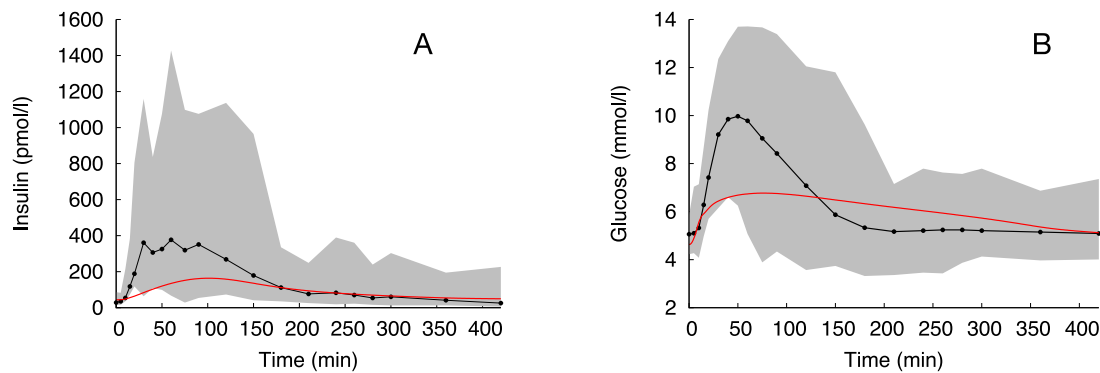
Fig. 5. Dynamics of metabolites in response to the meal test. Model fit vs experimental data from the study by Dalla Man *et al.* [36] during and after the meal test. The red line indicates the simulated concentration; the gray area represents the range of variability of the data, the black line represents the average concentrations. A: Glucose. B: Insulin.

Table 5
Estimated parameters of the glucagon/insulin model, along with their CV%.

Parameter	Value (CV%)	Units
k_1	0.01569 (5.4)	$pM^{-1}\ min^{-1}$
k_2	0.00014 (0.1)	$pM^{-1}\ min^{-1}$
k_3	3.08666 (15.6)	$pM^{-1}\ min^{-1}$
k_4	0.07095 (16.8)	$pM^{-1}\ min^{-1}$
D	0.00650 (9.1)	min^{-1}

and Panel E in Fig. 6,) and the increase of lactate (Panel D in Fig. 7) are generally slightly more pronounced for the model, and appear to produce an accumulation of these metabolites, because the return to the steady-state, although it is fast, appears with a certain delay compared to experimental data. In fact, the peak of the simulation at 300 min in Fig. 8 corresponds to the small peak at 180 min of the experimental data; the increasing trend at the end of the simulation corresponds to the peak at 300 min of the experimental value. Panel D in Fig. 4 reports the dynamics of simulated GLR, showing a delayed response of the decrease after the meal test and also an overestimation in the concentration values. The model-predicted increase for triglycerides appears underestimated in panel E in Fig. 4; although one must consider that experimental values have a very high standard deviation. Experimental data on triglycerides shows a return to the basal value that is slower than the one predicted by our model.

4. Discussion

The present study proposes a dynamic model of human energy metabolism, reflecting the integrated regulation of metabolism in the fasted and postprandial state, as well as during physical activity. We started from a multi-scale computational model able to describe fuel homeostasis in response to a bout of physical exercise previously proposed by our group [21]. We added a new working regime for the glucagon/insulin model to describe hormonal and metabolic changes due to ingestion of meals, expressed in terms of grams of carbohydrates, proteins, and fats, consumed by healthy subjects differing in gender, age, and anthropometric characteristics.

Eqs. (6) and (7) describe the mechanism of glucose regulation, and the return to the equilibrium, both in the case of diminution due to exercise or rising due to food intake. Thus, we decided to keep the same model. For the seek of simplicity, ease of use and code stability, the most convenient choice is to use the same model as the one proposed in our previous study, with different parameters. Summarizing, the introduction of this new working regime requires new estimates for the parameters (k_1, k_2, k_3, k_4, D) of the glucagon/insulin model in Eqs. (6) and (7), different from the ones used to only describe physical activity. They are obtained by fitting glucagon and insulin concentrations data

obtained from the study by Knop *et al.* [41], leading to the values reported in Table 5. The model simulation fits well the set of measured glucagon and insulin concentrations during the test study, also considering that five parameters are estimated using fifteen experimental data points, as evident in Fig. 3 and the good level of precision of the estimate is reflected by the low values for the CV%.

Our model slightly underestimates the plasma glucagon level, as reported in Fig. 3. The spanned range of glucagon concentration during glucose tolerance tests is part of the physiological inter-individual variability and is quite debated in the literature. As an example, in the studies by Gar and Manell [44,45], the values of the glucagon concentrations for healthy individuals are very similar to the one obtained by our estimation, with a suppression (with respect to the basal) of almost 5 pmol/l. Thus, we can state that our estimation is in line with other experimental observations of glucagon during glucose tolerance tests and is physiologically consistent and acceptable.

After the meal test, both insulin and glucagon concentrations return to their steady-state values $C_{I,0}$ and $C_{G,0}$, respectively. The correctly predicted return to the steady-state after meal periods (see Figs. 4, 5, 6) indicates that the model provides reliable results for this physiological condition. We chose to model the condition in between meals and exercise by using the same parameters as for the meal intake, but setting the food quantities to zero, as explained in Section 2.2.

The main novelty of this work lies in the modeling effort to integrate the description of the intake, stomach emptying, and absorption in the gastrointestinal tract of a complete mixed meal in the multi-scale model, thus allowing a better description of everyday real-life situations. The implementation of the model describing the dynamics of alanine (from proteins) and triglycerides (from fats) during meals needs the setting of proper parameters, described in section "Modeling food intake, stomach emptying and gut absorption" and listed in Table 2. One relevant question is, how sensitive the model is to these and other parameters. We considered that at the present first iteration of the model, it was not yet meaningful to perform an analysis of the sensitivity of the model to the choices made for the following reasons: (i) in the whole of the model, the parameters for the stomach emptying and absorption represent only a small subset of the overall parameter set; (ii) although we consider the model to be conceptually valid, the process of stomach emptying of mixed meals is a very complex one for which this work cannot provide a truly accurate description; any choice of parameter subsets to be varied for sensitivity analysis can be questioned for its physiological relevance; (iii) stomach emptying and nutrient absorption kinetics for identical meals vary widely between individuals and between different meals in the same individual, *e.g.*, evidenced by the analysis of postprandial glucose responses [46]. Therefore, the current model can only describe an average behavior across a population and a wide range of meals.
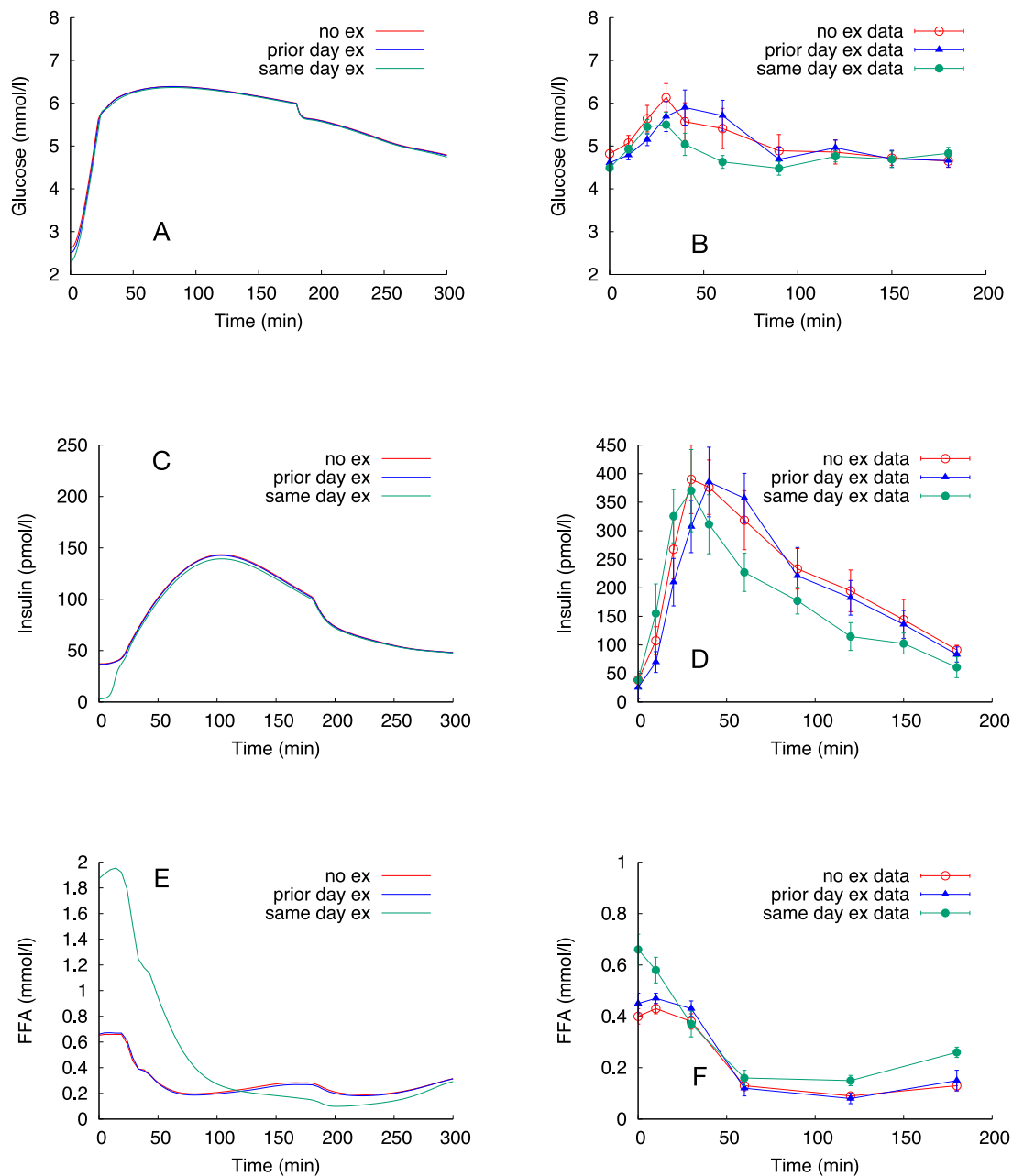
Fig. 6. Dynamics of metabolites in response to the meal test. Simulations and experimental data for the three trials from the study by Short *et al.* [37] during and after the meal test. In the trial indicated as "prior day ex", the subject performs a bout of aerobic exercise 17 h before consuming the mixed meal test. In the trial indicated as "same day ex", the subject performs a bout of aerobic exercise 1 h before consuming the mixed meal test. In the trial indicated as "no ex", the subject does not exercise before consuming the mixed meal test. Left panels: Model fits. The red lines represent the "no ex" trial, the green line reproduces the "prior day ex" trial, the blue line refers to the "same day ex" trial. Right panels: Experimental data. The filled circles represent the "same day ex" trial, the gray triangles indicate the "prior day ex" trial, the open circles correspond to the "no ex" trial. Panels A and B: Glucose. Panels C and D: Insulin. Panels E and F: Free Fatty Acids (FFA).

Due to a lack of experimental data in vivo, it was not feasible to validate that choices made for the parameterization of detailed aspects of the involved processes were realistic. It was however duly validated that the choices made led to realistic outcomes, using rate of appearance (Ra) data for the different macronutrients, as follows: the Ra of glucose, alanine, and triglycerides in the gut compartment, as explained in Eq. (3), compared to the experimental data, is shown in Fig. 9.

As evident from Fig. 9, the glucose Ra is properly modeled (Panel A): the peak of the simulated dynamics almost coincides both in time and amplitude with the data, being only slightly delayed in time. The model well describes the return to the basal state, even if the fall is less sharp. As previously stated in Section 2.1, we used alanine as a

representative for all amino acids derived from meal proteins. Since experimental data on alanine Ra are, to our knowledge, lacking, we used the venous blood Ra profile of phenylalanine, reported in the study by Groen and colleagues (see Panel B in Fig. 9) as a reference for amino acids Ra. Due to the fact that we compared two different amino acids, we introduced two different y-axes scales to account for the expected differences in the quantities; however, by comparing the two trends in Panel B, it is evident that the two Ra curves are similar in shape and timing. Note that the rate of appearance in our model is the flux of macronutrient metabolites into the gut compartment (see Eq. (3)) *i.e.,* before entering the mesenteric circulation and first-pass hepatic extraction, whereas the experimental data report the rate of appearance in the venous plasma. Regarding the validation of the Ra
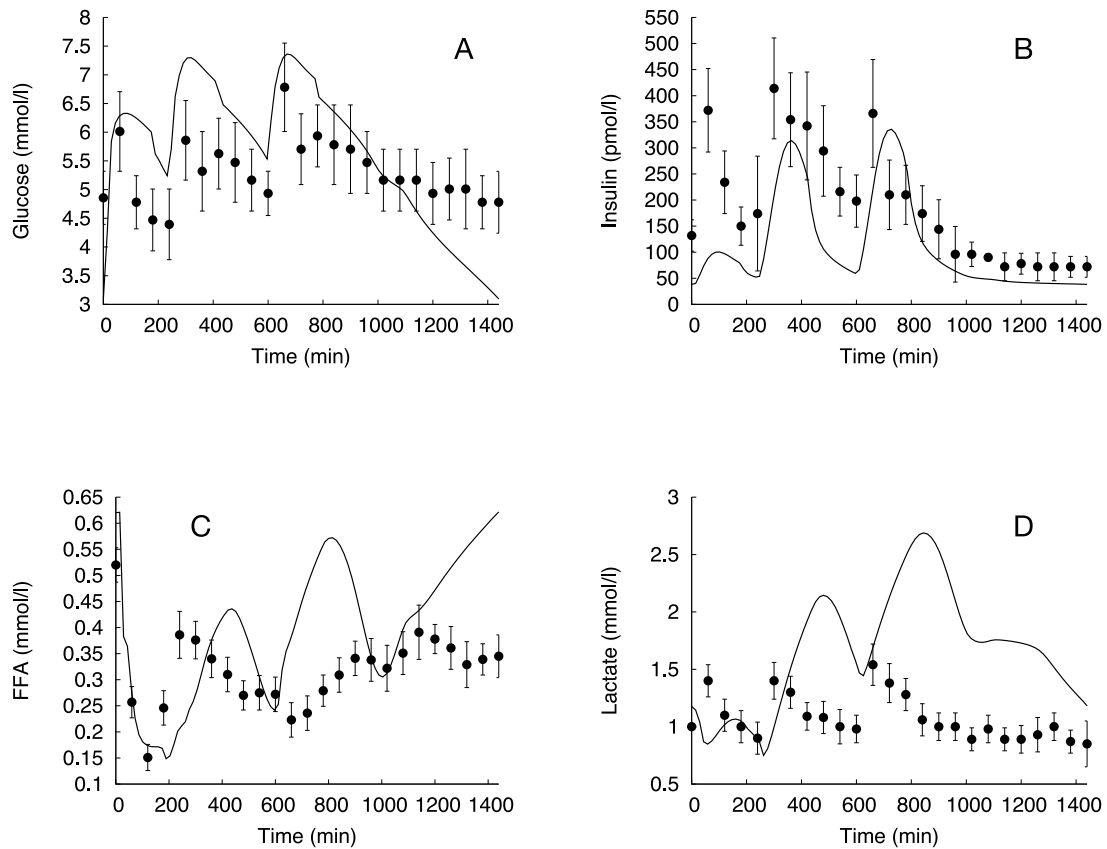
Fig. 7. Dynamics of metabolites in response to the meal test. Model fit (solid line) vs experimental data expressed as mean ± SE (circles with bars) during the one-day experiment from the study by Reaven *et al.* [38]. Panel A: glucose. Panel B: insulin. Panel C: Free Fatty Acids (FFA). Panel D: Lactate.
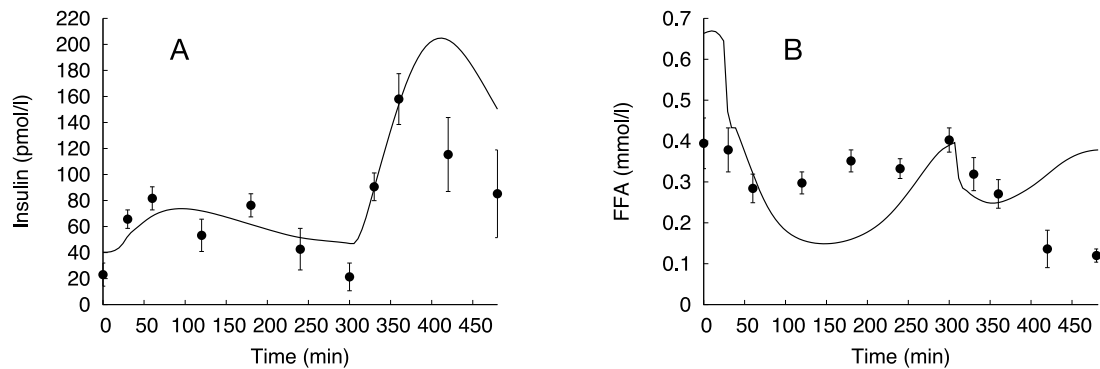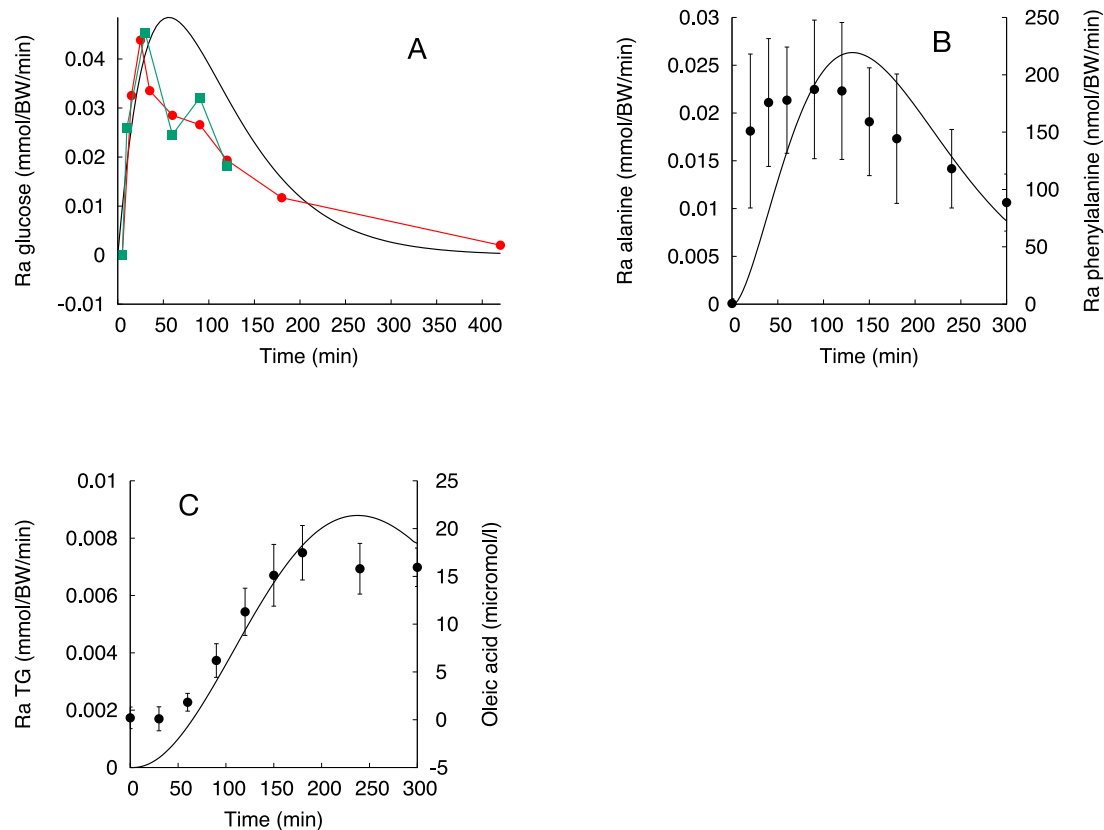

Fig. 8. Dynamics of metabolites in response to the meal test. Model fit (solid line) vs experimental data expressed as mean ± SE (circles with bars) from the study by Vors *et al.* [39] during and after the meal test for normal subjects. Panel A: Insulin. Panel B: Free Fatty Acids (FFA).

of triglycerides, we recall that we took oleic acid as representative of dietary triacylglycerol, as stated in Section 2.1. Vors and coworkers showed that the rate of influx of [13C]-labeled oleic acid from a meal with emulsified fat into plasma total fatty acids peaked at 180 min or later (see Fig. 2, Panel C in [39]). We obtained the same peak timing when simulating the test breakfast according to the paper by Vors, as evident in Fig. 9, Panel C. The use of different y-axes is dictated by necessity to indicate two different quantities: as already stated, the outcome of our model consists of a flux into the gut compartment, whereas the one showed by Vors is a venous plasma concentration profile. However, as in the case of alanine, we are interested in the correct timing and shapes of the curves even though the quantities are

different. Summarizing, based on the kinetics of the resultant overall appearance of the three individual macronutrients (glucose, amino acids, and fat) in plasma upon mixed meal tests described above, we consider that the choices made for the parameterization of stomach emptying and macronutrient absorption processes leads to realistic outcomes.

Our model predicts glucose concentration in the arterial blood compartment, whereas in the experimental setting, glucose is generally measured in the venous plasma. However, the difference between the two concentrations is reported to be negligible (approximately 3–5 mg/dl) [47]. With this consideration, the model properly captures the dynamics of the experimental glucose concentration data (see Panels A

Fig. 9. Rates of appearance in response to the meal stimulus. Model fit (solid line) vs experimental data expressed as mean ± SE (circles with errorbars) during and after the meal tests for normal subjects. Further information concerning the studies are available in Data regarding the experimental studies used for validation. Panel A: Glucose. Experimental data from the study by Dalla Man [36]. Green line: reduced protocol; red line: full protocol. Panel B: Alanine. The *y*-axis on the left refers to the simulation; the *y*-axis on the right refers to the experimental measures from the study by Groen [40]. Panel C: Triglycerides. The *y*-axis on the left refers to the simulation; the *y*-axis on the right refers to the experimental measures from the study by Vors [39].

in Figs. 4, 6, 7, Panel B in Fig. 5): the peaks are correctly located in time and also the amplitudes are quite well reproduced. In the post-absorptive state, the predicted glucose sometimes tends to fall lower than the experimental values before rising due to the meal test. In some cases the decrease after the test is less sharp than the ones of the measured values, but the steady state is well predicted in the case of a single meal. When considering the whole-day simulation with three meal as in Fig. 7, a drop in the glucose concentration at the end of the simulation is evident. However, the last peak is at 720 min, but the last experimental value is at 1440 min, thus meaning that the subject is fasted for more than 12 h. This could be an issue for the long-term simulations but, despite may happen, it is not a common scenario in the normal lifestyle, which is the case of interest of our study.

For what concerns the insulin dynamics, some simulations show a good agreement with the experimental tests: Panel A in Fig. 5 and Panels B in Fig. 4, 7 show a good fitting, with the simulated values in the range of variation of the experimental measures. However, lower values are predicted by the simulator in some cases as *e.g.,* in Panel C in Fig. 6, in which the peak is also delayed in time. In all the cases, the predicted values of insulin properly return to the steady-state after the meal tests.

When comparing the modeled FFA dynamics with the test values, the presence of a delay is evident; notwithstanding the model is able to provide outcomes in the same range of variability (see Panel C of Fig. 4 and Panel B of Fig. 8).

Panel D in Fig. 4 shows that the predicted concentrations of glycerol are quite overestimated, taking into consideration that the basal level of glycerol in adults is usually between 0.05 and 0.1mM [48]. As stated by Lin in [48], the kidney accounts for up to one fifth of the total glycerol

utilizing capacity of the body. Glycerol at a serum concentration of 1 mM can be completely cleared by the kidneys [49–52]. Since our computational model does not explicitly account for such a kidney contribution, this possibly explains our overestimation.

The simulations properly capture the trend of the lactate (Panel D in Fig. 7), even if the return to the steady-state is delayed.

The rise in the simulated arterial concentration of triglycerides in Panel E in Fig. 4 is underestimated during the meal test, and the immediate return to the steady-state predicted for the end of the meal period is at variance with experimental measures, which return to the state of equilibrium even later than the simulation window. We consider it a consequence of the fact that blood-tissue transport of TG is currently modeled as if it was a plasma soluble metabolite (*e.g.,* rapid tissue-plasma convergence to equilibrium), whereas actually triglyceride transport is effected by lipoproteins. This allows for much higher plasma concentrations of TG, and shows slower dynamics.

It is interesting to discuss the behaviour of the simulator when considering also the exercise session as in Fig. 6. Of note, for what concerns the glucose (Panels A, B), the model is able to reproduce a lower initial concentration for the trial in which the exercise is performed in the same day of the meal test. Even if the model generally overestimates the trends of FFA in all the three trials (Panels E, F), it properly captures the higher FFA concentration for the trial in which the exercise is performed in the same day of the meal test, as for the glucose.

We have previously shown that our model can reproduce the metabolic responses within a single day, in which different kinds of stimuli (*e.g.,* single meal or a single exercise session) are accounted for. This computational model can simulate even longer periods, such as
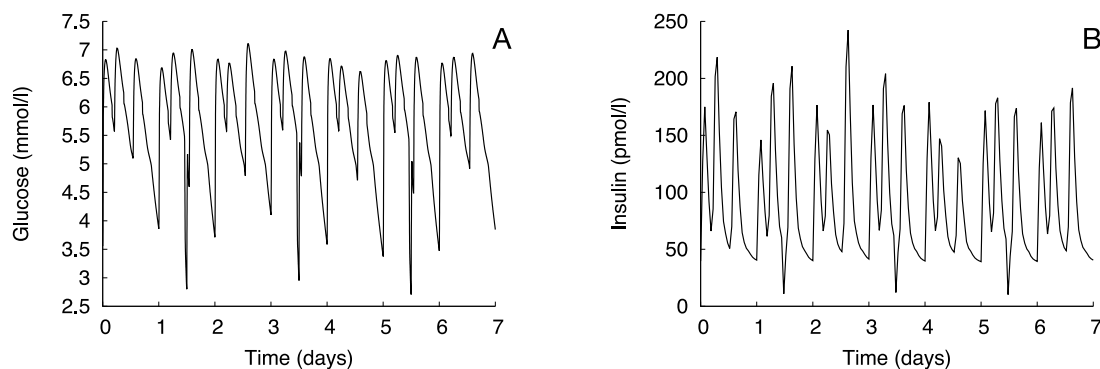
Fig. 10. Dynamics of metabolites in response to a one-week simulation. A: Glucose. B: Insulin.

weeks, owing to good numerical stability. As an example, in Fig. 10 a simulation of a full week period is provided for plasma glucose and insulin. Data regarding the physical characteristics of the virtual subject, the meals and the exercise scenarios are available in the supplemental files S1.txt and S2.txt. The meals scenarios are designed according to [53] and we hypothesized a fitness class "average" according to [23]. The exercise bouts are easily detectable in Fig. 10 and correspond to the three periods of moderate hypoglycemia and hypoinsulinemia. It is well-known that during exercise, subjects can experience periods of hypoglycemia; however, this drop in glucose concentration is limited and physiological [54].

Although some variations are evident in the fittings here shown, these differences may not have a significant impact from a clinical point of view. The most important result for us is to have realistic outcomes in the physiological ranges of acceptability, even if sometimes they are slightly delayed, over or underestimated. Our goal is to realize a model that permits to obtain realistic outcomes in order to generate virtual patients' populations, not to realize an artificial pancreas simulating the single individual's response.

5. Conclusions

Despite the mentioned shortcomings, the simulations are overall physiologically consistent and useful to describe the metabolic changes due to everyday life stimuli such as multiple mixed meals and variable periods of physical exercise, for different categories of subjects. Because of the large inter- and intra-individual variability of the physiological responses to these stimuli, a faithfully description of every person's situation cannot be reproduced. However, the modeling effort here presented provides a good compromise between detailing the involved processes and a system-level approach.

The model can represent a valid support to provide a cohort of virtual patients for clinical trial simulations, valuable tools for decision-making during the process of drug development, since it can represent realistic simulation scenarios, in which the patients must represent the target populations. The ability to perform long-term simulations with the possibility to input different quantities of food intake and exercise intensity and duration, allows representing the effects of various kinds of lifestyles on a set of virtual subjects differing in sex, age, height, weight, and fitness status. To our knowledge, this is the first attempt to describe the effects of macronutrients absorption, comprising also proteins and fats, in addition to glucose. Moreover, this is the first computational model that can achieve such a good level of detailing and customization so far released. Indeed, its use can span a broad spectrum of personalized medicine applications in the view of healthcare more based on the individual needs of the persons and can represent a useful tool for the generation of in-silico virtual patient populations.

CRediT authorship contribution statement

Maria Concetta Palumbo: Conception and design of the study, Software, Analysis and interpretation of the data, Visualisation, Drafting the article, Revising the article for final approval. **Albert A. de Graaf:** Conception and design of the study, Methodology, Analysis and interpretation of the data, Drafting the article, Revising the article for final approval. **Micaela Morettini:** Conception and design of the study, Methodology, Analysis and interpretation of the data, Drafting the article, Revising the article for final approval. **Paolo Tieri:** Revising the article for final approval. **Shaji Krishnan:** Methodology, Revising the article for final approval. **Filippo Castiglione:** Funding acquisition, Project administration, Analysis and interpretation of the data, Software, Visualization, Revising the article for final approval.

Declaration of competing interest

The authors declare that they have no known competing financial interests or personal relationships that could have appeared to influence the work reported in this paper.

Appendix A. Modeling glucose dynamics during an OGTT study

We estimated the parameters k_1, k_2, k_3, k_4 and D for the meal regime to fit the glucagon and insulin experimental data during the OGTT study by Knop in [41] (see Section 2.2). This procedure needs to know in advance the dynamics of glucose concentration, since glucose represents the input for the estimation procedure. Thus, we found a function fitting the glucose experimental data in the study by Knop, and representing the plasma glucose dynamics. We performed the fitting by using "cftool", a tool provided by MATLAB®(The MathWorks, Natick, MA, USA) to fit curves and surfaces to data and view plots. We used a Gaussian model was, namely

$$C_g(t) = a_1 \cdot e^{-(\frac{t-b_1}{c_1})^2} + a_2 \cdot e^{-(\frac{t-b_2}{c_2})^2} + a_3 \cdot e^{-(\frac{t-b_3}{c_3})^2} + a_4.$$

The coefficients a_1, a_2, a_3, a_4, b_1, b_2, b_3, c_1, c_2, c_3 are computed with 95% confidence bounds and are summarized in Table A.1.

The toolbox provides some methods to assess goodness of fit: confidence bounds, residual analysis, and goodness-of-fit statistics. The goodness of fit was evaluated in terms of Sum of Squares Due to Error (SSE), R-square, degrees of freedom adjusted R-square and Root

Table A.1

Estimated parameters. List of the values of the estimated parameters for the dynamics of arterial glucose concentration during an OGTT study [41].

Parameter	Value	Units
a_1	3.178	mmol
a_2	3.665	mmol
a_3	−1.774	mmol
a_4	5	mmol
b_1	34.3	min
b_2	61.24	min
b_3	57.07	min
c_1	24.67	min
c_2	49.3	min
c_3	144.8	min

Table A.2

Goodness-of-fit statistics.

Statistics	Value
SSE	0.5725
$R - square$	0.9916
$Adjusted\ R - square$	0.9848
$RMSE$	0.2393
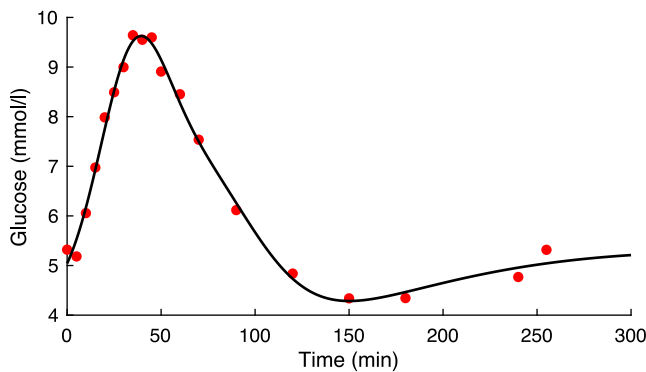
Fig. A.1. Glucose dynamics. Fit of the plasma glucose dynamics during an OGTT study [41].

Mean Squared Error (RMSE). Goodness-of-fit statistics is reported in Table A.2.

The resulting profile of glucose concentration is shown in Fig. A.1.

Appendix B. Data regarding the experimental studies used for validation

1. **van Schalkwijk** *et al.* [35]. Twelve male subjects were selected based on the waist-hip ratio (WHR). Patients with WHR < 1 were considered lower body obese (LBO), whereas subjects with WHR > 1 were considered as upper body obese (UBO). They were supplemented with 60g/day MCFA or linoleic acid for three weeks during which on average the subjects consumed about 105 g of fat daily. On day 20 (day before test day) subjects ate a standardized evening dinner which contained 548 kCal (50 g of CHO, 30 g of fat, 20 g of protein, and 5 g dietary fiber). On day 21, a test meal containing 40% of the total energy intake (1068 kcal) was provided. The macronutrient composition of the test meal was: 57 energy% from CHO; 32 energy% from fats; 12 energy% from proteins. Experimental data provided (courtesy of the authors) refers to this test meal. Blood samples were drawn at 0, 30, 60, 90 min and 2, 3, 4, and 6 h during and after the test meal.

2. **Dalla Man** *et al.* [36]. Plasma of 100 nondiabetic subjects were collected at 0, 5, 10, 15, 20, 30, 40, 50, 60, 75, 90, 120, 150, 180, 210, 240, 260, 280, 300, 360 and 420 min. The mixed meal consisted of 10 kcal/kg divided in 45% carbohydrate, 15% protein, and 40% fat. Two protocols sampling schedules were implemented, consisting in a different number of blood samples: full protocol consisting in 7 hours-21 samples and reduced protocol consisting in 2 hours-7 samples.

3. **Short** *et al.* [37] Eleven untrained young adults completed 3 trials. Two trials consisted of performing a 45-min aerobic exercise bout either 17-hours (Prior Day Ex) or 1-hour (Same Day Ex) before consuming the mixed meal test. The third trial consisted only in consuming the test meal (No Ex) without performing physical activity.

4. **Reaven** *et al.* [38]. Nine patients with normal glucose tolerance were fed an isocaloric (35 cal/kg) diet containing (as percentage of total calories) 17% protein, 40% fat, and 43% carbohydrate. Each meal, which was eaten at 8am, noon, and 6pm, contained 20, 40, and 40%, respectively, of the total daily calorie intake.

5. **Frayn** *et al.* [43]. Eight subject, after an overnight fast, received a meal containing 3.1 MJ, with 41% of calories from fat and 47% from carbohydrate.

6. **Vors** *et al.* [39]. Nine obese (OB) and nine normal weigh (NW) healthy subjects received a test breakfast consisting of 35.5 g of carbohydrates, 9.3 g of proteins and 41.4 of fats. A second meal was served 5 h after breakfast (91.5 g of carbohydrates, 35.7 g of proteins and 22.7 g of fats). For what concerns our study, we took into consideration the experimental data dealing with the spread fats.

7. **Groen** *et al.* [40]. Twenty healthy young adults received 20 g intrinsically [1-13C]-phenylalanine labeled protein.

Appendix C. Equations

An online version of the simulator, is available at https://kraken.iac.rm.cnr.it/T2DM.

C.1. Equations detailing the model of physical exercise

VO_{2max} is determined based on age, sex, and fitness status as described by Heyward in [23] (in place of the work rate WR) and the steady-state value for the oxygen consumption VO_2 is computed as

$$VO_2 = \frac{T_v \cdot VO_{2max}}{100}.$$

The original model by Kim [22] specifies the WR in Watts, thus we needed to express WR as a function of VO_2. To simulate different exercise modalities, we resorted to the metabolic equations provided by the American College of Sports Medicine (ACSM) [55] to estimate the oxygen consumption for five different exercise modalities.

$$WR(W) = \begin{cases} BW \cdot (VO_2 - 2 \cdot VO_{2,rest})/10.8 & \text{for leg cycling} \\ BW \cdot (VO_2 - VO_{2,rest})/18 & \text{for arm cycling} \end{cases}$$

where BW is the body weight, $VO_{2,rest}$ is the O_2 uptake at rest.

$$VO_2 = \begin{cases} VO_{2,rest} + 0.1 \cdot v + 1.8 \cdot v \cdot G & \text{for walking} \\ VO_{2,rest} + 0.2 \cdot v + 0.9 \cdot v \cdot G & \text{for running} \\ VO_{2,rest} + 0.2 \cdot F + 1.33 \cdot 1.8 \cdot H \cdot F & \text{for stepping} \end{cases}$$

in which v is speed expressed in m/min, G is the percent of slope expressed as a ratio, F is the stepping frequency expressed in steps/min and H is step height in meters. To obtain the WR for the last three categories of exercise, assuming a caloric equivalent for 1 liter of oxygen approximately 5 kcal [56,57], the following relationship is used to determine the Watt consumed per minutes for walking, running, and

stepping

$$WR(W) = VO_2 \cdot BW \cdot (t_{ex}^{end} - t_{ex}^{start}) \cdot 5 \cdot 10^{-3} \cdot 1.163$$

for walking, running, stepping

in which t_{ex}^{start} and t_{ex}^{end} are the beginning and the end of the exercise session expressed in minutes.

The kinetic of oxygen consumption is derived from Lenart, Roy and Parker [58,59]. Changes in oxygen consumption and the subsequent recovery phase are described in terms of %VO$_{2max}$ by means of the following linear first-order differential equation:

$$\frac{dPVO_{2max(t)}}{dt} = -0.8 \cdot PVO_{2max}(t) + 0.8 \cdot u(t)$$

in which $PVO_{2max}(t)$ is the suprabasal oxygen consumption, expressed as a percentage of the maximum value (%VO$_{2max}$) and $u(t)$ describes the input as a step function assuming value T_v for the entire duration of the exercise, that is

$$u(t) = \begin{cases} 0 & 0 \le t < t_{ex}^{start} \\ T_v & t_{ex}^{start} \le t \le t_{ex}^{end} \\ 0 & t > t_{ex}^{end}. \end{cases}$$

The model of epinephrine secretion and elimination (based on the %VO$_{2max}$ proposed by Kildegaard and colleagues in [60]) is adapted as follows

$$\frac{dC_{E(t)}}{dt} = \frac{1}{V_d} \cdot (f_1 + f_2 + f_3) \cdot BW - k \cdot C_E(t). \tag{10}$$

$C_E(t)$ is the epinephrine concentration, V_d is the volume of distribution, f_1 is a constant representing a basal epinephrine secretion, k is the epinephrine elimination constant.

$$f_2 = f_2(C_{a,g}(t)) = e_1 / \left(1 + e^{e_2 \cdot (Ca,g(t) - e_3)}\right)$$

$$f_3 = f_3(PVO_{2max}(t)) = d_1 / \left(1 + e^{d_2 \cdot (d_3 - PVO_{2max}(t))}\right).$$

The epinephrine elimination constant k is computed by imposing the steady-state condition in Eq (10), (*i.e.*, $T_v = 0$, $PVO_{2max}(t) = 0$, $C_{a,g}^* = 5$ mmol/l)

$$f_{2*} = f_2(C_{a,g}^*) = e_1 / \left(1 + e^{e_2 \cdot (Ca,g^* - e_3)}\right)$$

$$f_{3*} = f_3(0) = d_1 / \left(1 + e^{d_2 \cdot d_3}\right).$$

$$k = \frac{BW}{V_d \cdot C_{E,0}} \cdot (f_1 + f_2^* + f_3^*).$$

C.2. Equations detailing the glucagon/insulin model

The dynamics of glucagon and insulin during the meal period is given by the following differential equations:

$$\frac{dC_I}{dt} = C_I(t) \cdot \left[\psi \cdot [h - k_3 \cdot (C_G(t) - C_{G,0}) - k_4 \cdot (C_I(t) - C_{I,0}) - k_5 \cdot (C_E(t) - C_{E,0})] - D\right]$$

$$\frac{dC_G}{dt} = C_G(t) \cdot \left[\phi \cdot [h - k_1 \cdot (C_G(t) - C_{G,0}) - k_2 \cdot (C_I(t) - C_{I,0})] - D\right]$$

$$\phi = \begin{cases} 1 & C_{a,glc} < 2.5 \\ 1 - (C_{a,glc} - 2.5)^2 / 25 & 2.5 \le C_{a,glc} \le 7.5 \\ 0 & C_{a,glc} > 7.5 \end{cases}$$

$$\psi = \begin{cases} 0 & C_{a,glc} < 2.5 \\ 1 - (C_{a,glc} - 7.5)^2 / 25 & 2.5 \le C_{a,glc} \le 7.5 \\ 1 & C_{a,glc} > 7.5 \end{cases}$$

C.3. Equations detailing the model of the food digestion

The gastric emptying rates for nutrient glucose (*glu*), alanine (*ala*) and triglycerides (*tg*) are:

$$G_{emp,glu}(t) = D_{glu} \cdot \beta_{glu} \cdot K_{e,glu}^{\beta_{glu}} \cdot t^{(\beta_{glu} - 1)} \cdot e^{-(K_{e,glu} \cdot t)^{\beta_{glu}}}$$

Table C.1
Parameters for the model of the epinephrine dynamics.

Parameter	Value	Units
V_d	15	l
k	0.2746	pM^{-1} min^{-1}
d_1	0.47	nmol^{-1} min^{-1} kg^{-1}
d_2	0.1	
d_3	82	%VO_2
e_1	0.360	nmol kg^{-1} min^{-1}
e_2	5	nmol of ADR kg^{-1} min^{-1} mmol^{-1} of glucose l^{-1}
e_3	2.94	mmol l^{-1}

Table C.2
Estimated parameters of the glucagon/insulin model.

Parameter	Value for meal	Value for exercise	Units
k_1	0.01569	0.2707	pM^{-1} min^{-1}
k_2	0.00014	0.0535	pM^{-1} min^{-1}
k_3	3.08666	0.1507	pM^{-1} min^{-1}
k_4	0.07095	0.0309	pM^{-1} min^{-1}
k_5	1	$3.6 \cdot 10^{-5}$	pM^{-1} min^{-1}
D	0.00650	0.1	min^{-1}
h	D/0.75	D/0.75	min^{-1}

Table C.3
Parameters used to model the meal intake. List of model parameters for stomach emptying and absorption of glucose (glu), alanine (ala) and triglycerides (tg).

Parameter	Value for OGTT	Value for mixed meal	Units
β_{glu}	1.23 [27]	1.05	
β_{ala}		1.6	
β_{tg}		2.2	
$K_{e,glu}$	0.011 [27]	0.0164	min^{-1}
$K_{e,ala}$		0.0086	min^{-1}
$K_{e,tg}$		0.0042	min^{-1}
$K_{abs,glu}$	0.231 [27]	0.021	min^{-1}
$K_{abs,ala}$		0.013	min^{-1}
$K_{abs,tg}$		0.017	min^{-1}
$F_{abs,glu}$	0.9 [27]	0.9	
$F_{abs,ala}$		0.95	
$F_{abs,tg}$		0.95	

$$G_{emp,ala}(t) = D_{ala} \cdot \beta_{ala} \cdot K_{e,ala}^{\beta_{ala}} \cdot t^{(\beta_{ala} - 1)} \cdot e^{-(K_{e,ala} \cdot t)^{\beta_{ala}}}$$

$$G_{emp,tg}(t) = D_{tg} \cdot \beta_{tg} \cdot K_{e,tg}^{\beta_{tg}} \cdot t^{(\beta_{tg} - 1)} \cdot e^{-(K_{e,tg} \cdot t)^{\beta_{tg}}}$$

The equations describing first-order kinetics of glucose absorption and rate of appearance are given below (see Tables C.1–C.3):

$$dy_{glu}(t)/dt = -K_{abs,glu} \cdot y_{glu}(t) + G_{emp,glu}(t)$$

$$dy_{ala}(t)/dt = -K_{abs,ala} \cdot y_{ala}(t) + G_{emp,ala}(t)$$

$$dy_{tg}(t)/dt = -K_{abs,tg} \cdot y_{tg}(t) + G_{emp,tg}(t)$$

$$Ra_{glu}(t) = F_{abs,glu} \cdot K_{abs,glu} \cdot y_{glu}(t)$$

$$Ra_{ala}(t) = F_{abs,ala} \cdot K_{abs,ala} \cdot y_{ala}(t)$$

$$Ra_{tg}(t) = F_{abs,tg} \cdot K_{abs,tg} \cdot y_{tg}(t)$$

Appendix D. Supplementary data

Supplementary material related to this article can be found online at https://doi.org/10.1016/j.compbiomed.2023.107158.

References

[1] C. Lachat, S. Otchere, D. Roberfroid, A. Abdulai, F.M.A. Seret, J. Milesevic, G. Xuereb, V. Candeias, P. Kolsteren, Diet and physical activity for the prevention of noncommunicable diseases in low-and middle-income countries: A systematic policy review, PLoS Med. 10 (6) (2013) e1001465.

[2] T. Vos, C. Allen, M. Arora, R.M. Barber, Z.A. Bhutta, A. Brown, A. Carter, D.C. Casey, F.J. Charlson, A.Z. Chen, et al., Global, regional, and national incidence, prevalence, and years lived with disability for 310 diseases and injuries, 1990–2015: A systematic analysis for the Global Burden of Disease Study 2015, Lancet 388 (10053) (2016) 1545–1602.

[3] WHO, Global report on diabetes, 2021, URL: https://www.who.int/en/news-room/fact-sheets/detail/diabetes. (Accessed 29 June 2021).

[4] International Diabetes Federation, IDF diabetes Atlas, 2023, URL: https://diabetesatlas.org/idfawp/resource-files/2021/07/IDF_Atlas_10th_Edition_2021.pdf. (Accessed 15 March 2023).

[5] H. Sun, P. Saeedi, S. Karuranga, M. Pinkepank, K.e.a. Ogurtsova, IDF diabetes Atlas: Global, regional and country-level diabetes prevalence estimates for 2021 and projections for 2045, Diabetes Res. Clin. Pract. 183 (2022) 109119.

[6] S. Chatterjee, K. Khunti, M.J. Davies, Type 2 diabetes, Lancet 389 (10085) (2017) 2239–2251.

[7] M. Sagner, A. McNeil, P. Puska, C. Auffray, N.D. Price, L. Hood, C.J. Lavie, Z.-G. Han, Z. Chen, S.K. Brahmachari, B.S. McEwen, M.B. Soares, R. Balling, E. Epel, R. Arena, The P4 health spectrum – A predictive, preventive, personalized and participatory continuum for promoting healthspan, Prog. Cardiovasc. Dis. 59 (5) (2017) 506–521.

[8] I.I. Adamu, E.J.D. Garba, Y. Haruna, Mathematical model for the dynamics of glucose regulatory system under the combined use of dieting and physical exercise, Ozean J. Appl. Sci. 5 (3) (2012) 229–241.

[9] B. Topp, K. Promislow, G. deVries, R.M. Miura, D.T. Finegood, A model of beta-cell mass, insulin, and glucose kinetics: Pathways to diabetes, J. Theoret. Biol. 206 (4) (2000) 605–619, URL: http://dx.doi.org/10.1006/jtbi.2000.2150.

[10] D. Svitra, I. Basov, R. Vilkyté, Modelling of glycaemia dynamics: Impact of physical exercises, Nonlinear Anal. Model. Control 15 (2) (2010) 213–232.

[11] M.D. Breton, Physical activity-the major unaccounted impediment to closed loop control, J. Diabetes Sci. Technol. 2 (1) (2008) 169–174.

[12] C. Dalla Man, M.D. Breton, C. Cobelli, Physical activity into the meal glucose-insulin model of type 1 diabetes: In silico studies, J. Diabetes Sci. Technol. 3 (1) (2009) 56–67.

[13] N.P. Balakrishnan, L. Samavedham, G.P. Rangaiah, Personalized hybrid models for exercise, meal, and insulin interventions in type 1 diabetic children and adolescents, Ind. Eng. Chem. Res. 52 (36) (2013) 13020–13033.

[14] N. Resalat, J. El Youssef, N. Tyler, J. Castle, P.G. Jacobs, A statistical virtual patient population for the glucoregulatory system in type 1 diabetes with integrated exercise model, PLoS One 14 (7) (2019) e0217301.

[15] M.J. Islam, A.S.M.L. Hoque, Virtual diabetic patient with physical activity dynamics, Comput. Methods Programs Biomed. (2021) 106485.

[16] J. Deichmann, S. Bachmann, M. Pfister, G. Szinnai, H.-M. Kaltenbach, A comprehensive model of glucose-insulin regulation including acute and prolonged effects of physical activity in type 1 diabetes, 2021, BioRxiv.

[17] J. Sarkar, G. Dwivedi, Q. Chen, I.E. Sheu, M. Paich, C.M. Chelini, P.M. D'Alessandro, S.P. Burns, A long-term mechanistic computational model of physiological factors driving the onset of type 2 diabetes in an individual, PLoS One 13 (2) (2018) e0192472.

[18] H. Kurata, Virtual metabolic human dynamic model for pathological analysis and therapy design for diabetes, Iscience 24 (2) (2021) 102101.

[19] U. Morbiducci, G. Di Benedetto, A. Kautzky-Willer, M.A. Deriu, G. Pacini, A. Tura, Identification of a model of non-esterified fatty acids dynamics through genetic algorithms: The case of women with a history of gestational diabetes, Comput. Biol. Med. 41 (3) (2011) 146–153.

[20] M. Morettini, M. Palumbo, C. Göbl, L. Burattini, Y. Karusheva, M. Roden, G. Pacini, A. Tura, Mathematical model of insulin kinetics accounting for the amino acids effect during a mixed meal tolerance test, Front. Endocrinol. 13 (2022).

[21] M. Palumbo, M. Morettini, P. Tieri, F. Diele, M. Sacchetti, F. Castiglione, Personalizing physical exercise in a computational model of fuel homeostasis, PLoS Comput. Biol. 14 (4) (2018) e1006073.

[22] J. Kim, G.M. Saidel, M.E. Cabrera, Multi-scale computational model of fuel homeostasis during exercise: Effect of hormonal control, Ann. Biomed. Eng. 35 (1) (2007) 69–90.

[23] V.H. Heyward, A.L. Gibson, Advance Fitness Assessment and Exercise Prescription, Human Kinetics, Champain, IL, 2014.

[24] A.C. Hindmarsh, P.N. Brown, K.E. Grant, S.L. Lee, R. Serban, D.E. Shumaker, C.S. Woodward, SUNDIALS: Suite of nonlinear and differential/algebraic equation solvers, ACM Trans. Math. Softw. 31 (3) (2005) 363–396.

[25] S.D. Cohen, A.C. Hindmarsh, CVODE, a stiff/nonstiff ODE solver in C, Comput. Phys. 10 (2) (1996) 138–143.

[26] C. Brignoli, J. Kinsella, J. Weihrauch, Comprehensive evaluation of fatty acids in foods. V. Unhydrogenated fats and oils, J. Am. Diet. Assoc. 68 (3) (1976) 224–229.

[27] C. Dalla Man, M. Camilleri, C. Cobelli, A system model of oral glucose absorption: Validation on gold standard data, IEEE Trans. Biomed. Eng. 53 (12 Pt 1) (2006) 2472–2478.

[28] J.D. Elashoff, T.J. Reedy, J.H. Meyer, Analysis of gastric emptying data, Gastroenterology 83 (6) (1982) 1306–1312.

[29] O. Couturier, C. Le Rest, J. Gournay, M. Pourdehnad, B. Bridji, A. Turzo, Y. Bizais, Gastric emptying of solids: Estimates of lag phase and constant emptying times, Nucl. Med. Commun. 21 (7) (2000) 665–675.

[30] G. Tougas, Y. Chen, G. Coates, W. Paterson, C. Dallaire, P. Paré, M. Boivin, A. Watier, S. Daniels, N. Diamant, Standardization of a simplified scintigraphic methodology for the assessment of gastric emptying in a multicenter setting, Am. J. Gastroenterol. 95 (1) (2000) 78.

[31] G. Tougas, E.Y. Eaker, T.L. Abell, H. Abrahamsson, M. Boivin, J. Chen, M.P. Hocking, E.M. Quigley, K.L. Koch, A.Z. Tokayer, et al., Assessment of gastric emptying using a low fat meal: Establishment of international control values, Am. J. Gastroenterol. 95 (6) (2000) 1456–1462.

[32] J. Calbet, D. MacLean, Role of caloric content on gastric emptying in humans, J. Physiol. 498 (Pt 2) (1997) 553–559.

[33] The engineering toolbox, 2010, [online] https://www.engineeringtoolbox.com/density-materials-d_1652.html [Accessed 25 June 2022].

[34] E. Weber, H.-J. Ehrlein, Relationships between gastric emptying and intestinal absorption of nutrients and energy in mini pigs, Digest. Dis. Sci. 43 (6) (1998) 1141–1153.

[35] D.B. van Schalkwijk, W.J. Pasman, H.F. Hendriks, E.R. Verheij, C.M. Rubingh, K. van Bochove, W.H. Vaes, M. Adiels, A.P. Freidig, A.A. de Graaf, Dietary medium chain fatty acid supplementation leads to reduced VLDL lipolysis and uptake rates in comparison to linoleic acid supplementation, PLoS One 9 (7) (2014).

[36] C. Dalla Man, M. Campioni, K.S. Polonsky, R. Basu, R.A. Rizza, G. Toffolo, C. Cobelli, Two-hour seven-sample oral glucose tolerance test and meal protocol: Minimal model assessment of β-cell responsivity and insulin sensitivity in nondiabetic individuals, Diabetes 54 (11) (2005) 3265–3273.

[37] K.R. Short, L.V. Pratt, A.M. Teague, The acute and residual effect of a single exercise session on meal glucose tolerance in sedentary young adults, J. Nutr. Metab. 2012 (2012).

[38] G.M. Reaven, C. Hollenbeck, C.-Y. Jeng, M.S. Wu, Y.-D.I. Chen, Measurement of plasma glucose, free fatty acid, lactate, and insulin for 24 h in patients with NIDDM, Diabetes 37 (8) (1988) 1020–1024.

[39] C. Vors, G. Pineau, L. Gabert, J. Drai, C. Louche-Pélissier, C. Defoort, D. Lairon, M. Désage, S. Danthine, S. Lambert-Porcheron, et al., Modulating absorption and postprandial handling of dietary fatty acids by structuring fat in the meal: A randomized crossover clinical trial, Am. J. Clin. Nutr. 97 (1) (2013) 23–36.

[40] B.B. Groen, A.M. Horstman, H.M. Hamer, M. De Haan, J. Van Kranenburg, J. Bierau, M. Poeze, W.K. Wodzig, B.B. Rasmussen, L.J. Van Loon, Post-prandial protein handling: You are what you just ate, PLoS One 10 (11) (2015) e0141582.

[41] F.K. Knop, T. Vilsbøll, J.J. Madsbad, T. Krarup, Inappropriate suppression of glucagon during OGTT but not during isoglycaemic I.V. glucose infusion contributes to the reduced incretin effect in type 2 diabetes mellitus, Diabetologia 50 (2007) 797–805.

[42] E.R. Carson, L. Finkelstein, C. Cobelli, Mathematical Modeling of Metabolic and Endocrine Systems: Model Formulation, Identification, and Validation, John Wiley & Sons, INC., 605 THIRD AVE., NEW YORK, NY 10158, USA, 394, 1983.

[43] K.N. Frayn, S.W. Coppack, S.M. Humphreys, M.L. Clark, R.D. Evans, Periprandial regulation of lipid metabolism in insulin-treated diabetes mellitus, Metabolism 42 (4) (1993) 504–510.

[44] C. Gar, M. Rottenkolber, V. Sacco, S. Moschko, F. Banning, N. Hesse, D. Popp, C. Hübener, J. Seissler, A. Lechner, Patterns of plasma glucagon dynamics do not match metabolic phenotypes in young women, J. Clin. Endocrinol. Metab. 103 (3) (2018) 972–982.

[45] H. Manell, J. Staaf, L. Manukyan, H. Kristinsson, J. Cen, R. Stenlid, I. Ciba, A. Forslund, P. Bergsten, Altered plasma levels of glucagon, GLP-1 and glicentin during OGTT in adolescents with obesity and type 2 diabetes, J. Clin. Endocrinol. Metab. 101 (3) (2016) 1181–1189.

[46] D. Zeevi, T. Korem, N. Zmora, D. Israeli, D. Rothschild, A. Weinberger, O. Ben-Yacov, D. Lador, T. Avnit-Sagi, M. Lotan-Pompan, et al., Personalized nutrition by prediction of glycemic responses, Cell 163 (5) (2015) 1079–1094.

[47] E. Cengiz, W.V. Tamborlane, A tale of two compartments: Interstitial versus blood glucose monitoring, Diabetes Technol. Ther. 11 (S1) (2009) S–11.

[48] E. Lin, Glycerol utilization and its regulation in mammals, Annu. Rev. Biochem. 46 (1) (1977) 765–795.

[49] J. Robinson, E. Newsholme, The effects of dietary conditions and glycerol concentration on glycerol uptake by rat liver and kidney-cortex slices, Biochem. J. 112 (4) (1969) 449–453.

[50] P. Kruhøffer, O.I. Nissen, Handling of glycerol in the kidney, Acta Physiol. Scand. 59 (3) (1963) 284–294.

[51] D. Zilversmit, E.L. McCandless, Fate of intravenously administered glycerol, Proc. Soc. Exp. Biol. Med. 95 (4) (1957) 755–757.

[52] E. Strack, D. Biesold, Glycerin blood level & metabolism in rabbits, Zeitschrift Fur Die Gesamte Experimentelle Medizin 130 (6) (1959) 547–555.

[53] M.D. Mifflin, S.T. St Jeor, L.A. Hill, B.J. Scott, S.A. Daugherty, Y.O. Koh, A new predictive equation for resting energy expenditure in healthy individuals, Am. J. Clin. Nutr. 51 (2) (1990) 241–247.

[54] J.W. Porter, R.J. Pettit-Mee, S.T. Ready, Y. Liu, G. Lastra, A. Chockalingam, N.C. Winn, L. Clart, J.A. Kanaley, Post meal exercise may lead to transient hypoglycemia irrespective of glycemic status in humans, Front. Endocrinol. 11 (2020) 578.

[55] American College of Sports Medicine, et al., ACSM's Guidelines for Exercise Testing and Prescription, Lippincott Williams & Wilkins, Philadelphia, PA, 2013.

[56] W.D. McArdle, F.I. Katch, V.L. Katch, Essentials of Exercise Physiology, Lippincott Williams & Wilkins, Philadelphia, PA, 2006.

[57] I. Kohlstadt, Scientific Evidence for Musculoskeletal, Bariatric, and Sports Nutrition, CRC Press, Boca Raton, FL, 2006.

[58] P.J. Lenart, R.S. Parker, Modeling exercise effects in type 1 diabetic patients, in: IFAC Proc World Congress on Automatic Control, 2002.

[59] A. Roy, R.S. Parker, Dynamic modeling of exercise effects on plasma glucose and insulin levels, J. Diabetes Sci. Technol. 1 (3) (2007) 338–347.

[60] J. Kildegaard, T.F. Christensen, M.D. Johansen, J. Randløv, O.K. Hejlesen, Modeling the effect of blood glucose and physical exercise on plasma adrenaline in people with type 1 diabetes, Diabetes Technol. Ther. 9 (6) (2007) 501–507.